Supporting Information

Yu et al. 10.1073/pnas.1108270109

SI Materials and Methods

Animal Preparation. Ferrets (postnatal day 40–45; Marshall Farms) were premedicated with atropine (0.04 mg/kg, i.m.) before anesthesia. Anesthesia was induced with a combination of ketamine (25 mg/kg, i.m.) and xylazine (2 mg/kg, i.m.). The animals were intubated, and anesthesia was maintained with isoflurane (2–2.5% during surgery) in O_2. Lidocaine (2%) was applied to incision areas. A small craniotomy (2 mm × 4 mm) was performed to expose the primary visual cortex, and the dura was deflected. A glass pipette (tip diameter of approximately 20 μm) filled with genetically modified Sindbis virus carrying the EGFP gene (1) was inserted into the cortex, and the virus was slowly injected at the depths of 500 and 200 μm under the pia, through a microdrive-connected plunger. Each injection contained 0.25 μL of virus and lasted for 5 min. A chronic window (transparent coverglass on top of 2% agarose) was implanted above the exposed cortex, and all the incision points, exposed skull, and window edges were sealed with dental cement. A light five-hole metal plate was securely glued to the skull close to the window, allowing stable imaging at the same focal plane at different time points by screwing the plate to the imaging table (for both intrinsic and two-photon imaging). For analgesia, buprenorphine (0.1 mg/kg, i.m.) was administered immediately after surgery, as well as 12, 24, and 36 h after surgery and thereafter if necessary. Amoxicillin (10 mg/kg, i.m.) was injected once per day to prevent infection. After the animal was ambulating, it was sent back to the cage for 2 d to allow time for gene expression.

Two days later, intrinsic signal optical imaging and two-photon imaging were performed through the chronic window. The animals were intubated and anesthetized with isoflurane (2% for two-photon imaging, 1.5% for optical imaging). The EKG, expired CO_2, and temperature were continuously monitored to ensure adequate levels of anesthesia. The eyelid of the contralateral eye was sutured following the initial baseline imaging, under continued anesthesia (the level of isoflurane was increased to 2.0–2.5%). For analgesia, buprenorphine (0.1 mg/kg, i.m.) was administered following surgery but before anesthetic gases were discontinued. Vetropolycin was applied topically on the sutured skin to prevent infection. The animals usually woke up in 10 min after the anesthesia was discontinued. When they were fully awake, the animals were engaged in play for 3 to 6 h to ensure that they experienced their visual environment before the next imaging session. Similar procedures were followed for visual experience recovery when the sutured eyelid was opened. Animals in the monocular deprivation (MD) group always received the same sequence: (*i*) initial imaging followed by eye suture; (*ii*) eye-reopening and reimaging 6 h later; and (*iii*) a final recovery imaging session 24 h later. Two control animals were imaged in the same manner except without lid suture. An additional two control animals were reimaged after a 24-h interval followed by a 6-h interval as a result of constraints on imaging and surgery time. There were no differences in spine loss or gain observed between these two sets of control animals at the different imaging intervals, and numbers were pooled for statistical comparison with MD animals. Animals whose window became "cloudy," degrading the quality of the two-photon imaging at any time point, were discarded from the study.

Optical Imaging. In brief, red light (630 nm) was used to illuminate the cortical surface, and the change of reflectance was captured by a video acquisition system (Optical Imaging) during the presentation of visual stimuli (Cambridge Systems). Monocularly presented drifting gratings (four orientations, spatial frequency of 0.125 cycles per degree) were used to obtain ocular dominance (OD) maps, with 5 s of visual stimuli and 7 s of rest. Images were captured 2 s before and during the stimulation period at the frame rate of 1 Hz. Retinotopic and/or spatial frequency maps were also obtained to delineate the border between area 17 (V1) and 18 (V2). All analysis was carried out in area 17.

To obtain a single condition orientation map, the averages of five frames during stimulation (i.e., F1) and two frames before stimulation (i.e., F0) were subtracted and divided [(F0 − F1) / F0]. The averages of all orientation single-condition maps for each eye represent monocular eye response maps. Ipsilateral (i.e., nondeprived) and contralateral (i.e., deprived) eye response maps were subtracted to generate the OD map, and OD index (ODI) was further corrected from the control bone area. Higher values represent more nondeprived eye domination, and 0 represents binocularly driven areas. The average ODI of ferret primary visual cortex is significantly contralateral eye-dominated, as described previously (2, 3).

Two-Photon Imaging. A custom-made two-photon laser-scanning microscope was used for in vivo imaging (4). The microscope consists of a modified Fluoview confocal scanhead (Olympus) and a Ti:S laser providing 100-fs pulses at 80 MHz at a wavelength of 920 nm (Tsunami; Spectra-physics) pumped by a 10-W solid-state source (Millenia; Spectra-physics). Fluorescence was detected by using photomultiplier tubes (HC125-02; Hamamatsu) in whole-field detection mode. The window was initially identified under whole-field fluorescence illumination, and areas with superficial dendrites were identified by using a 20× 0.95 NA lens (IR2; Olympus). Spiny dendrites were further identified under digital zoom (10×), and spines 50 to 200 μm below the pial surface were studied. Image acquisition was accomplished by using Fluoview software. Multiple Z-stacks were acquired (1 μm apart at magnification of 10× for spines, 5 μm at magnification of 1× for dendrites and cell bodies).

Images were exported to Matlab for further analysis. To determine spine persistence over time, 3D image stacks were aligned over multiple time points and spines were identified manually. A spine was considered to be persistent if it could be identified in two optical sections and was longer than 0.5 μm. As an additional precaution, we averaged the fluorescence of all pixels within a spine (outlined by the observer), and spines were counted as present only if this average was higher than the average plus 1 SE of the background fluorescence (measured adjacent to the spine; Fig. 1*F*). For reidentification of dendritic spines between imaging sessions, a spine was allowed 0.5 μm lateral movement along the dendrite with respect to landmarks such as other spines and axon terminals. Spines that were displaced by less than 0.5 μm between imaging sessions were considered to be persistent (or reappearing within the same location). All spine loss and gain is reported with respect to the preceding imaging session. Spines were characterized into classes based on their lengths, spine head diameters, and neck diameters (5). Analysis was carried out blindly with respect to visual deprivation and OD preference, and identical criteria were strictly followed in all data sets.

ODI of Spines. Blood vessel maps were obtained during intrinsic signal optical imaging (546 nm, focused at the pial surface) and two-photon imaging (800 × 600 μm at 1×, multiple Z-stacks 5 μm apart within top 100 μm). The Z-stack images were averaged to provide an outline of the shadowed blood vessel prints, and the

blood vessel map was rotated and shifted accordingly to align with the intrinsic signal vessel map. Each spine site (80 × 60 μm at 10×) was marked in the collapsed 1× two-photon blood vessel map and linked to the intrinsic signal blood vessel map, and then to the intrinsic signal OD map. The spine site occupied only 6 × 4 pixels in the OD map (pixel size, 14 μm), and the ODI of these pixels were averaged, serving as the ODI of the spine site.

Simulation of MD Effects: Binocularly Independent and Dependent Models. The experimental maps from the deprived and nondeprived eye were used in the simulation. In the binocularly independent model, in which each eye is proposed to affect responses independent of the other, every pixel of the deprived eye response map was reduced by a fixed percentage (40%), and the nondeprived response map was increased by 10%, based on the estimates from our experimental data. Thus, after simulation, the ODI would be nondeprived*1.1 − deprived*0.6. In the binocularly dependent competitive model, in which the effect of deprivation depends on interaction between the two eyes, the ODI with the greatest absolute value (i.e., from the most monocularly dominated pixel) was adopted to normalize the ODI value of all the pixels to generate a binocularity index:

$$\mathrm{BI} = 1 - \mathrm{abs}(\mathrm{ODI}/\mathrm{M}) \qquad \textbf{[S1]}$$

In this case, 1 represents pure binocular drive, and the smaller the BI, the greater the monocularity, with 0 representing pure monocular drive. M represents the most monocularly dominated pixel. Next, deprived and nondeprived eye response maps were modified by 25% according to the binocularity index-deprived map [deprived*(1 − BI*0.25] and nondeprived map [ND*(1 + BI*0.25)]. This manipulation emphasizes a shift in binocular areas, which should allow the greatest interaction between the two eyes while limiting plasticity in monocular areas.

1. Jeromin A, Yuan LL, Frick A, Pfaffinger P, Johnston D (2003) A modified Sindbis vector for prolonged gene expression in neurons. *J Neurophysiol* 90:2741–2745.
2. Yu H, Farley BJ, Jin DZ, Sur M (2005) The coordinated mapping of visual space and response features in visual cortex. *Neuron* 47:267–280.
3. Issa NP, Trachtenberg JT, Chapman B, Zahs KR, Stryker MP (1999) The critical period for ocular dominance plasticity in the Ferret's visual cortex. *J Neurosci* 19:6965–6978.
4. Majewska A, Yiu G, Yuste R (2000) A custom-made two-photon microscope and deconvolution system. *Pflugers Arch* 441:398–408.
5. Oray S, Majewska A, Sur M (2004) Dendritic spine dynamics are regulated by monocular deprivation and extracellular matrix degradation. *Neuron* 44:1021–1030.

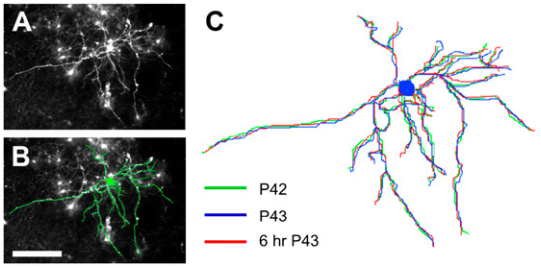

Fig. S1. Stable dendritic structure in control animals over 2 d. (*A*) Collapsed image showing a cell with its processes. (*B*) Outline (green) of the dendritic tree of this cell. (*C*) Overlay of the dendritic tree of the same cell at three different time points shows stable morphology. (Scale bar: 100 μm.)

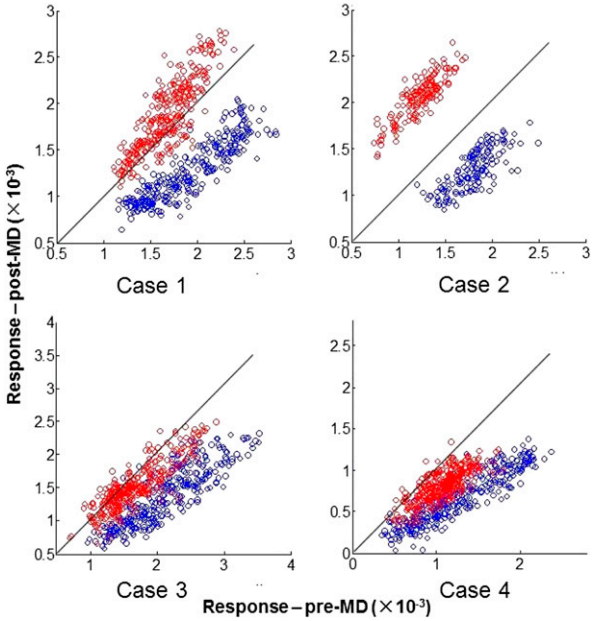

Fig. S2. Scatter plots of responses of both eyes before and after MD. For each eye in each ferret, post-MD responses of one of every 100 pixels chosen at random from the map were plotted against their pre-MD responses. Red represents the nondeprived eye and blue represents the deprived eye.

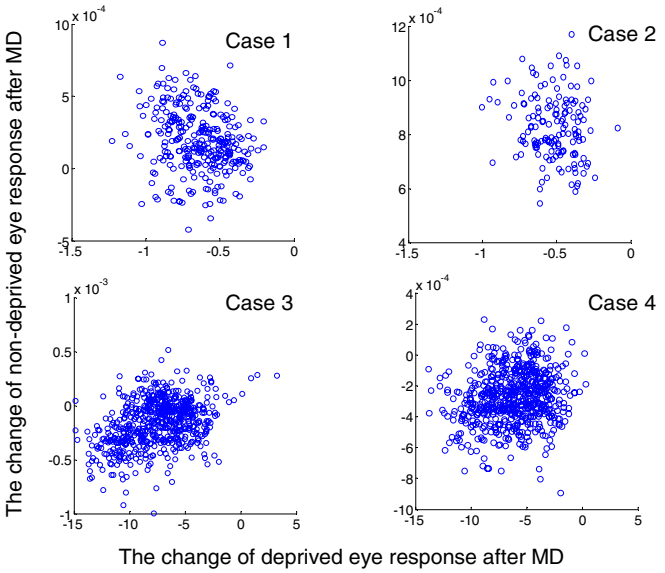

Fig. S3. Lack of close correlation between changes in deprived and nondeprived eyes. For each of four animals, the change in the nondeprived eye was plotted against the change observed in the deprived eye following MD. Notice the large scatter in the plots.

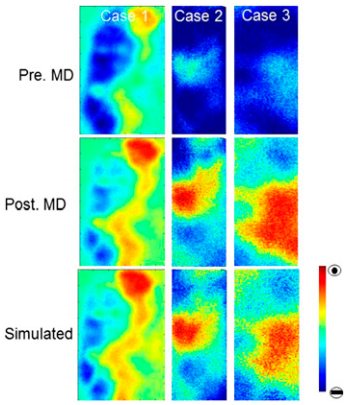

Fig. S4. Simulated OD maps match the experimental OD maps after MD. Comparison of experimental data and simulated data based on a global shift after MD, applied independently for each eye for three additional cases.

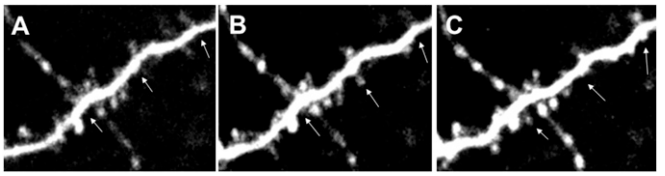

Fig. S5. Spine gain during the recovery period occurs largely at new dendritic locations. Image of a dendritic section before MD (*A*), after MD (*B*), and after recovery (*C*). Arrows indicate locations were spines are lost and gained between imaging sessions. Note that, in this case, two spines appear during the recovery period (*C*) at locations that did not have spines before MD. The middle arrow shows a spine that was gained during the MD period and then subsequently lost after recovery.

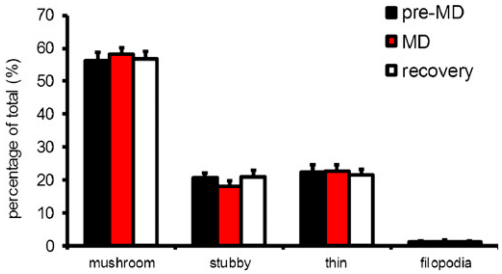

Fig. S6. MD and recovery from MD do not elicit large-scale morphological changes in stable dendritic spines. The proportions of mushroom spines, stubby spines, thin spines, and filopodia were determined at different time points including pre-MD, after 6 h MD, and at 1 day recovery. Spine types and distributions appeared similar across conditions in both animals (923 spines were monitored starting in the pre-MD condition; n = 2 animals).

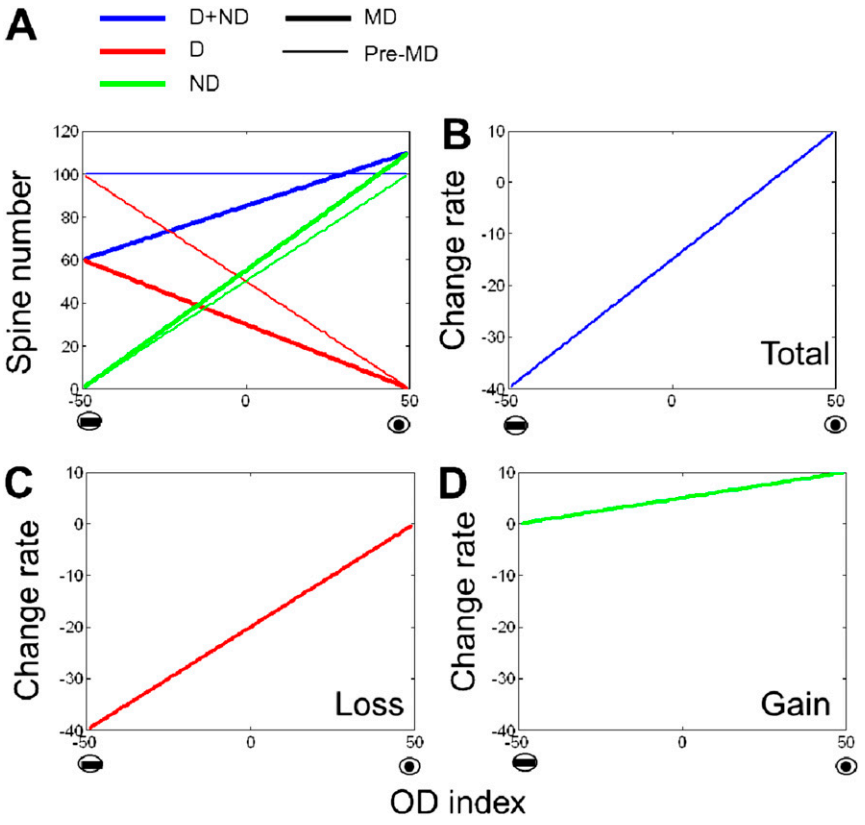

Fig. S7. Prediction of spine turnover based on a global shift, applied independently for each eye, after MD. (*A*) A global shift after MD, based on independent influences of each eye, predicts greater total spine loss in the deprived eye-dominated region. In this ideal model, the ODI determines the number of spines driven by the deprived eye (red) and nondeprived eye (green). For example, in a pure deprived eye-dominated region (i.e., ODI = −50), all the spines (N = 100) are deprived eye-driven, and in a binocular region (i.e., ODI = 0), 50 spines are deprived eye-driven and the other 50 are nondeprived eye-driven. Thus, at any location within the cortex, there are always 100 total spines (deprived plus nondeprived) in the pre-MD condition (thin blue line). After MD, a 40% reduction of deprived eye-driven spines (thick red) and 10% increase of nondeprived eye-driven spines (thick green) was globally applied, and this imbalanced shift causes a positive correlation between the total spine number and ODI: the more deprived eye-dominated the cortical region is, the greater the total spine loss (thick blue line). (*B–D*) In terms of change rates (number of spines lost or gained divided by total number of spines in the pre-MD condition), the predicted model data are analogous to measurements in Fig. 5 *B–D*, and can be directly compared with the experimental data.

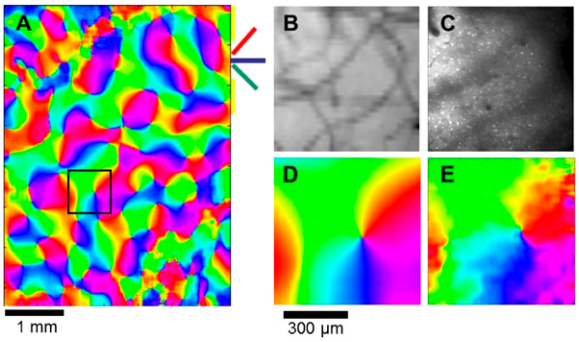

Fig. S8. Correlation between neuropil tuning observed by using two-photon calcium imaging and global tuning observed by using intrinsic signal imaging. (*A*) Orientation tuning map obtained by using intrinsic signal imaging in young ferret visual cortex. Boxed area is shown in *B*–*E*. (*B*) Vessel map used to locate the same area in the two-photon microscope. (*C*) Two-photon image shows many neurons labeled by using extracellular injections of Oregon green 488 BAPTA-1, a calcium indicator. (*D*) Intrinsic signal map of boxed area in *A*. (*E*) Orientation map obtained by using two-photon imaging of calcium responses of neuropil only (cell bodies were excluded from the analysis).